Journal of Medicinal Chemistry

Article

pubs.acs.org/jmc

Identification of Small Molecule Inhibitors of the HIV-1 Nucleocapsid–Stem-Loop 3 RNA Complex

Douglas M. Warui and Anne M. Baranger*

Department of Chemistry, 361 Roger Adams Laboratory, University of Illinois, 600 South Mathews Avenue, Urbana, Illinois 61801, United States

Supporting Information

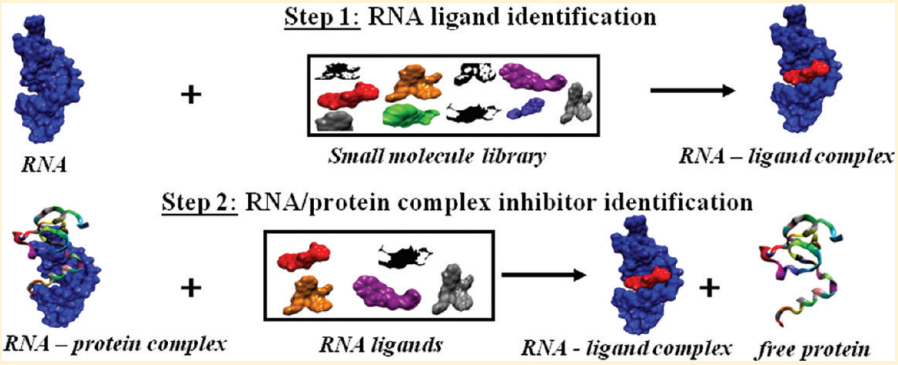

ABSTRACT: Stem-loop 3 RNA (SL3) in ψ-RNA is a highly conserved motif in different strains of HIV-1 and serves as a principle determinant for viral packaging. Viral encapsulation is critical for viral replication, and disruption of the nucleocapsid–ψ-RNA complex interferes with viral replication. We have used SL3 RNA as a target for identification of small molecule inhibitors of the interactions of nucleocapsid protein (NCp7) and ψ-RNA. We report the use of computational and high-throughput screening approaches to identify 16 compounds that bind SL3 RNA with micromolar affinities. Among the identified ligands, two molecules, compounds **7** and **17**, bind with higher affinity to SL3 RNA than to double- and single-stranded RNAs. Four of the 16 SL3 RNA ligands inhibit interactions between SL3 RNA and NCp7 with micromolar inhibition constants. In general, the identified SL3 ligands have simple molecular structures and low molecular weights and are, therefore, possible lead compounds for the development of ligands that target the elements of ψ-RNA of HIV-1 with high affinity and specificity.

INTRODUCTION

The large number of RNA–protein interactions that have been reported and the extensive, diverse functions and structures of RNA molecules suggest RNA–protein complexes as powerful therapeutic targets.[2] RNA is characterized by regions of unpaired bases or mismatched base pairs that allow the RNA to fold into distinct, complex secondary and tertiary structures that form unique pockets and deep grooves suitable for interactions with other RNAs, proteins, and small molecules.[3−8] Targeting such RNA structures in biologically relevant ribonucleoprotein complexes provides opportunities for controlling RNA function.

Although the usefulness of RNA as a small molecule target has been demonstrated by various classes of antibiotics that target specific regions of the prokaryotic ribosome[1,9−12] and many milestones have been accomplished in the past decade toward targeting RNA with small molecules,[13] there are few examples of the identification of small RNA ligands that inhibit RNA–protein interactions.[14−30] In some cases, such efforts have been hindered by the fact that RNA ligands that bind with high affinity to RNA targets often do so without inhibiting proteins from binding.[19,26,30] Perhaps as a result, oligomers of RNA binding molecules are often the focus of studies identifying RNA ligands that disrupt RNA–protein complexes.[14−16,25] However, small molecule inhibitors of the HIV Tat-TAR and Rev-RRE complexes and of the large binding interface formed between an RRM of the U1A protein and RNA have been identified.[18−20,26,29] The inhibition of the MBNL1-poly(CUG) complex by pentamidine and a triaminotriazine–acridine conjugate is relevant to the investigations reported here because MBNL1 is a zinc finger protein similar to the nucleocapsid protein.[23,24] Inhibition of RNA–protein complexes by RNA ligands can be biologically effective. For example, the destabilization of complexes formed between proteins and RNA G-quadruplex structures by bisquinolino derivatives inhibits translation,[28] and the destabilization of the IRE-IRP complex by yohimbine controls protein biosynthesis.[17]

The major packaging domain of HIV-1 retrovirus, called the ψ-recognition element, is located at the 5′ untranslated region of the unspliced HIV-1 genomic RNA and comprises four stem-loops SL1–4 (Figure 1).[31−33] Selective and efficient

Received: June 14, 2011
Published: April 5, 2012

dx.doi.org/10.1021/jm2007694 | J. Med. Chem. 2012, 55, 4132–4141

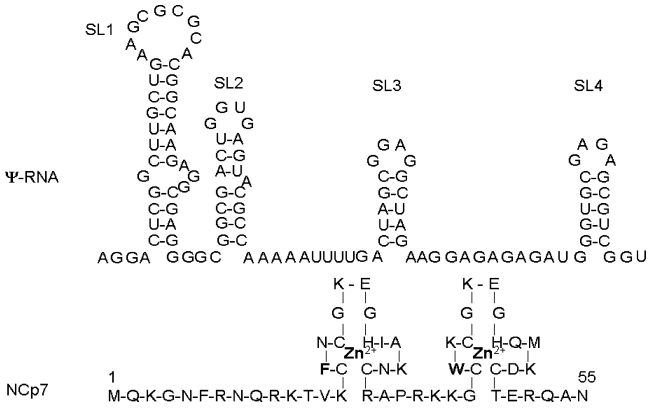

Figure 1. Sequence of HIV-1 genomic RNA packaging signal (ψ-RNA) with its characteristic stem-loop structures abbreviated SL1 through SL4. Shown is the amino acid sequence of nucleocapsid domain (NCp7) of HIV-1 Gag, including its two CCHC-zinc finger structures. Aromatic amino acids within the zinc fingers (bold) make specific interactions with ψ-RNA particularly with the GGAG tetraloop of SL3.

encapsulation of the viral genome results from specific recognition of the highly structured ψ-recognition element by the protein NCp7 using two zinc fingers.[34−43] SL3, a GGAG hairpin, is highly conserved among different strains of HIV-1, specifically interacts with NCp7, and is a principle packaging determinant.[37] Inhibition of the interactions between NCp7 and ψ-RNA should interfere with viral replication. In fact, antisense RNA targeted to ψ-RNA elements, ψ-RNA decoys, and zinc ion ejection has been reported to demonstrate antiviral activity.[44−48] A recent study reported an optimized peptide ligand of ψ-RNA that demonstrated antiviral activity in vivo.[33] A screen of known RNA ligands showed that some of those that bind SL1−4 of ψ-RNA are able to destabilize the complex formed between NCp7 and RNA.[30] SL3 RNA is not a target of current anti-HIV therapeutics, and thus, new small molecule ligands that target SL3 and disrupt interactions with NCp7 protein could act as lead compounds for novel anti-HIV agents.

We previously used computational docking strategies to identify new RNA ligands that bind to GNRA and GGAG tetraloops.[49,50] Experimental characterization of the identified compounds revealed nine RNA ligands that bound the GGAG stem loop in SL3 RNA of ψ-RNA with micromolar affinities.[49] Here we report the use of virtual and high-throughput screening strategies to identify 16 additional small molecules that bind to SL3 RNA with micromolar affinities. Two of the newly identified ligands selectively bind to SL3 RNA compared to either double- or single-stranded RNA. All of the small molecules from these two studies have been evaluated as inhibitors of the interactions between SL3 RNA and NCp7 protein, and four of the molecules identified by computational screening are effective inhibitors of the interactions between SL3 and NCp7. Thus, computational screening has successfully identified four molecules, previously not known to be RNA ligands, that bind to SL3 RNA and destabilize the SL3 RNA−NCp7 complex with micromolar inhibition constants.

RESULTS AND DISCUSSION

Screening SL3 Ligands for Inhibition of the NCp7−SL3 RNA Complex. We previously reported the identification of 27 potential ligands for SL3 RNA by computational docking the NCI diversity set library to SL3 RNA.[49] In our current studies, we screened these molecules for their ability to destabilize the complex formed between NCp7 protein and SL3 RNA. The equilibrium dissociation constant of the NCp7−SL3 RNA complex was determined to be 36 ± 11 nM using gel mobility shift assays, which is consistent with a previous report (Figures 2 and 3).[43] Each of the 27 ligands from the NCI

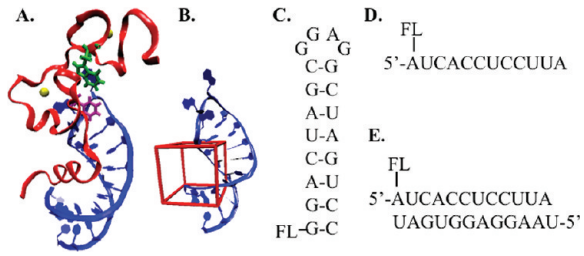

Figure 2. (A) NMR structure of SL3 RNA in complex with nucleocapsid protein (PDB code 1A1T). RNA is in blue, and protein backbone is in red.[59] The positions of the zinc atoms in the NCp7 zinc knuckles are represented by yellow spheres. Phe16 and Trp37 residues that mediate specific interactions with the elements of ψ-RNA are highlighted in purple and green, respectively. (B) Docking site (red box) on SL3 RNA (blue) depicting the site where compounds were docked in the virtual screening process. Parts C, D, and E are 5′-fluorescein labeled sequences of SL3, single-stranded RNA, and double-stranded RNA, respectively, used in the binding studies.

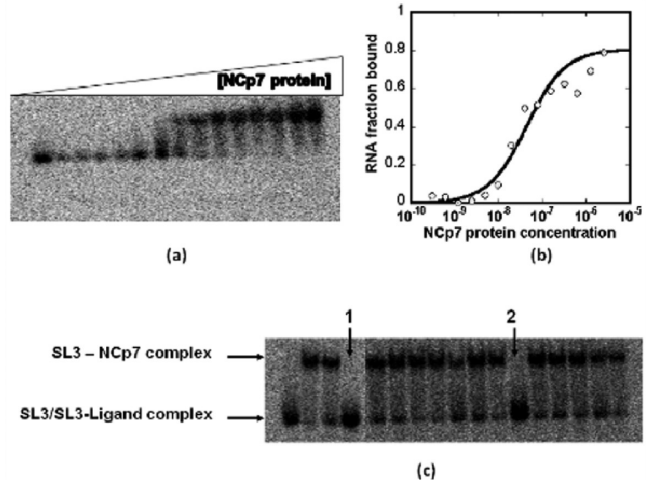

Figure 3. Electrophoretic gel mobility shift assay for the measurement of the equilibrium dissociation constant of NCp7 to SL3 RNA and initial inhibition screening results for identification of inhibitors **1** and **2**. (a) Representative gel showing binding of NCp7 to SL3 RNA. The concentration of NCp7 protein was varied from 1.5 nM to 12.5 μM. (b) Representative binding curve derived from plotting the fraction RNA bound as a function of NCp7 protein concentration. (c) Initial inhibition screening results for the identification of compounds **1** and **2** as inhibitors of SL3−NCp7 interactions.

diversity set library was added to a final concentration of 1 mM to the NCp7−SL3 RNA complex, incubated for 1 h, and evaluated using gel mobility shift assays (Figure 3). These studies revealed two compounds, **1** and **2**, that inhibit NCp7−SL3 RNA interactions (Figure 4). Unfortunately the identity of **2**, obtained from the NCI diversity set, could not be confirmed by mass spectrometry or NMR spectroscopy. Therefore, we performed a virtual similarity screening search, described in the next section, to identify structurally similar compounds that

dx.doi.org/10.1021/jm2007694 | J. Med. Chem. 2012, 55, 4132−4141

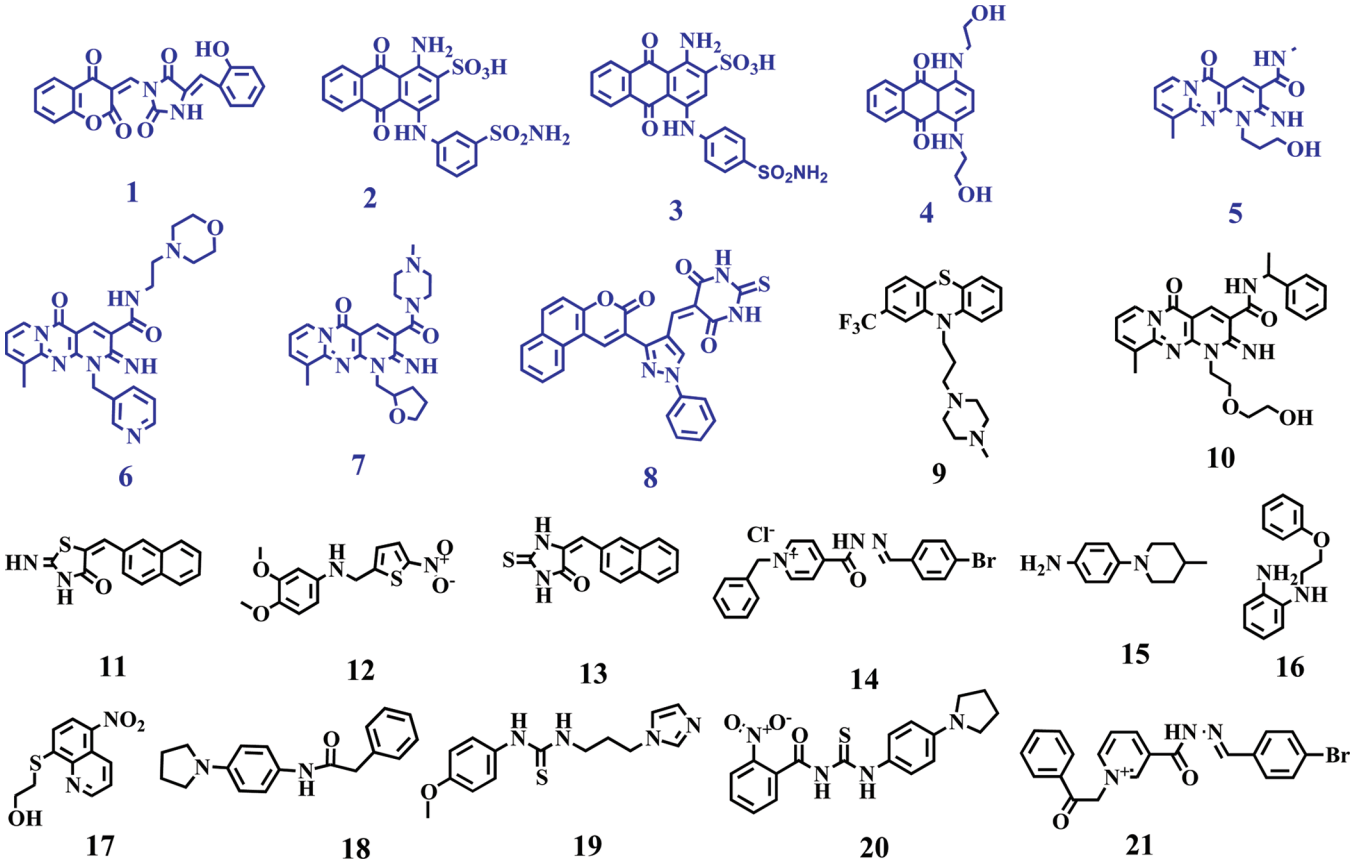

Figure 4. Chemical structures of hit molecules. Compounds **1**–**8** (blue) were identified through computational screening processes (Supporting Information Figure 1a), while compounds **9**–**21** (black) were identified through the high-throughput screening (Supporting Information Figure 1b).

may also have affinity for SL3 RNA and inhibit NCp7–SL3 RNA interactions.

Identification of SL3 Ligands Using Computational Docking. We performed two similarity screens to identify molecules similar to **2**. First, we used SciFinder Scholar to search for compounds that had ≥95% similarity to **2** and were commercially available. From this approach, we identified **3** (Figure 4). In a second similarity screen (Supporting Information Figure 1a), we utilized the ChemBridge library of 700 000 compounds because it is large, contains compounds with high molecular structural diversity, and hit compounds can be purchased in pure form for experimental evaluation. This approach led to the identification of 62 compounds with 50% or greater similarity to **2** based on a Tanimoto score that is obtained from a set of structural descriptors defined by the program.

Because previous studies from our group and others have suggested that the use of molecular docking can be a useful predictor of RNA–ligand interactions,[49−57] we used the program AutoDock to evaluate the binding to SL3 RNA of **3** and the 62 selected compounds identified in the similarity searches. AutoDock uses a Lamarckian genetic search algorithm and employs an exhaustive scoring function that includes desolvation, hydrogen bonding, ligand torsional, van der Waals, and electrostatic energies.[58] The structure of the SL3 RNA bound to the NCp7 protein was chosen as the target for computational docking (Figure 2).[59] We used the same docking site as we used in our previously reported screen of the NCI diversity set.[49] This docking site was defined as the major groove region proximal to the flexible loop area, which is the site of interaction of a 3_{10} helix of NCp7 and is proximal to the binding site of the N-terminal zinc knuckle of the NCp7.[59]

The analysis of the docking results revealed 18 compounds (17 compounds from the ChemBridge library and compound **3** from Scientific Exchange, Inc.) that were predicted to bind SL3 RNA with binding energies of ≤−7.0 kcal mol^{-1}. Because of the importance of water solubility, the six compounds (**3**–**8**, Figure 4) with log P(O/W) ≤ 1 were selected for experimental evaluation. The structures predicted by AutoDock of the complexes formed between SL3 RNA and **1** and **3**–**8** are shown in Figure 5. Compounds **1**, **5**, **7**, and **8** are predicted to interact with the junction region between the loop and the major groove of SL3 RNA, the binding site of the N-terminus 3_{10} helix of NCp7. In contrast to **1**, **5**, **7**, and **8**, compounds **3** and **4** were predicted to bind to the loop region of the RNA.

Identification of SL3 Ligands by High-Throughput Screening. In addition to the computational screening strategy described above, we performed a high-throughput screen to identify ligands for SL3 RNA in the 150 000-compound ChemBridge library. The compounds in this library were selected using over 60 computational methods at ChemBridge to ensure structural diversity and druglikeness. The high-throughput screening process used in these studies is outlined in Supporting Information Figure 1b. SL3 RNA was 5′-end labeled with fluorescein. The compounds were screened for binding to SL3 RNA by monitoring the change in fluorescence signal (490 nm excitation, 515 nm emission) upon addition of each compound to a final concentration of 1 mM. To remove false hits from the identified compounds, a repeat screen was performed on the selected hit compounds, followed by

dx.doi.org/10.1021/jm2007694 | J. Med. Chem. 2012, 55, 4132–4141

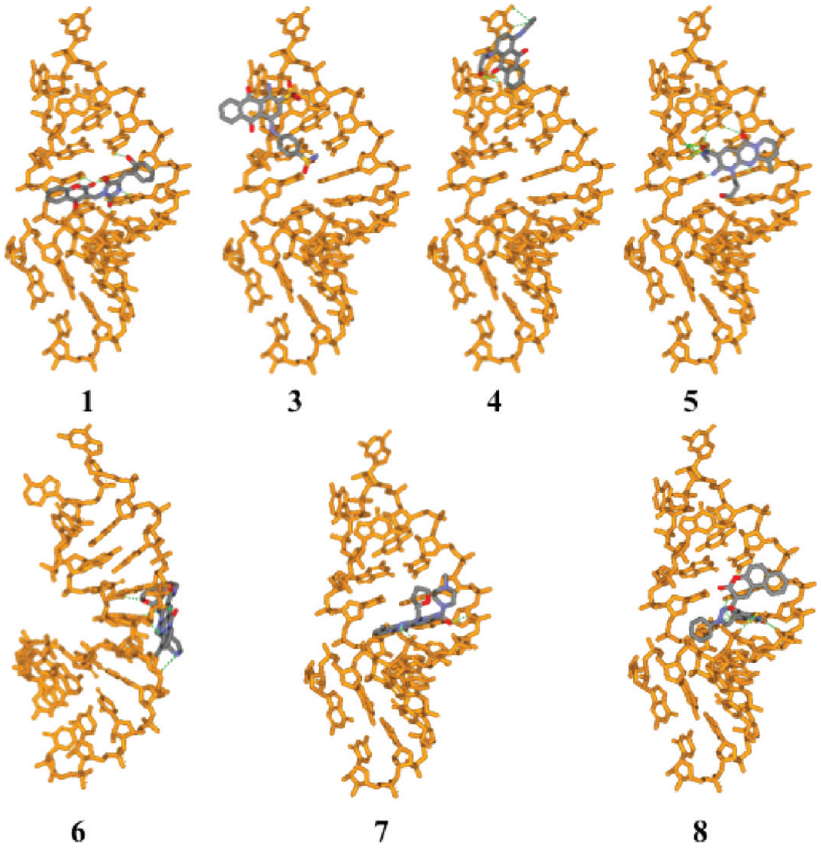

Figure 5. Best binding poses predicted by AutoDock for the seven molecules (**1** and **3**–**8**) identified by computational methods as ligands for SL3 RNA. The small molecules are represented with sticks, while the RNA is displayed with balls and sticks (orange). Intermolecular hydrogen bond interactions are shown with dashed green lines.

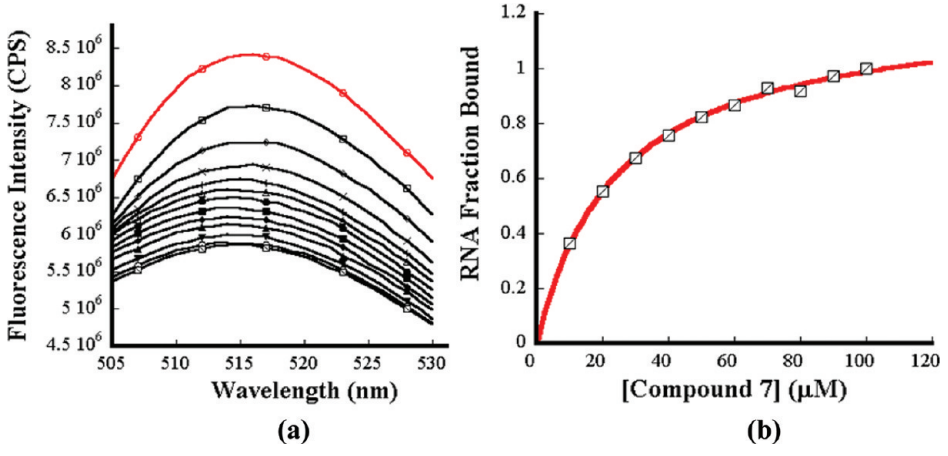

Figure 6. (a) Representative graph of decreasing fluorescence intensity of fluorescein-labeled SL3 RNA (25 nM) upon addition of increasing concentrations (10–100 μM) of **7**. The initial fluorescence emission spectrum of the RNA is in red. (b) Representative plot of the fraction of SL3 RNA bound as a function of the concentration of **7**. The data were fit with eq 1 to determine the apparent dissociation constant assuming 1:1 binding of the ligand to SL3 RNA.

screening of the resulting hit molecules against a solution containing fluorescein alone. By use of this procedure, 95 compounds were identified as potential SL3 binders. We further limited the selected molecules by considering only molecules with log P(O/W) $\leq$ 3. By use of this criterion, 13 compounds were retained (Figure 4, compounds **9**–**21**).

Binding Affinity of Selected Ligands for SL3 RNA. The equilibrium binding affinities of ligands identified by computational docking and high-throughput screening to SL3 RNA were determined by monitoring changes of the fluorescence intensity of 5′-fluoroscein-labeled SL3 RNA as a function of ligand concentration. Each assay was accompanied by a control experiment in which the ligand was titrated into a fluorescein solution in order to exclude the possibility of signal changes resulting from the ligand interacting directly with fluorescein or from ligand precipitation. A representative plot of the fluorescence of the labeled RNA as a function of ligand concentration is shown in Figure 6a. In these experiments, the

dx.doi.org/10.1021/jm2007694 | J. Med. Chem. 2012, 55, 4132–4141

fluorescein-labeled RNA was excited at 490 nm and emission was monitored from 505 to 530 nm. The emission at 517 nm was used to calculate dissociation constants (K_D). For all ligands, the fraction of RNA bound was calculated by dividing the difference between the sample and initial fluorescence intensities by the difference between the final and initial fluorescence intensities. The fraction of RNA bound was then plotted against the concentration of each ligand as shown in Figure 6b. The data of most compounds were fit using eq 1,[60,61] which assumes a 1:1 binding stoichiometry. Because the data obtained from **1** binding to RNA were not fit well with a 1:1 binding model, these data were fit using eq 2, which assumes a 2:1 cooperative model (Table 1).

Table 1. Summary of the Experimentally Determined Apparent Dissociation Constants of the Complexes Formed between SL3 RNA and Compounds Identified through Both the Computational and High-Throughput Screening Strategies[a]

compd	K_D (μM)
1	163 ± 2
3	11 ± 5[b]
4	1.1 ± 0.1
5	3.5 ± 0.3
6	5.0 ± 0.3
7	10 ± 5
8	68[b]
9	1.7 ± 0.2
10	4.5 ± 0.9
11	11 ± 2
12	11.1 ± 0.1
13	13.2 ± 0.3
14	33 ± 3
15	44 ± 6
16	51
17	90 ± 10
18–21	no binding

[a]Dissociation constants were determined from fluorescence binding measurements except where otherwise noted. Errors are the standard deviation of at least three independent measurements. [b]Dissociation constants were determined using ITC, and errors are the standard deviation of two measurements. Only the dissociation constants for the strongest binding sites are listed.

$$(F - F_0)/(F_f - F_0) = (a[\text{ligand}])/(K_D + [\text{ligand}]) \quad (1)$$

$$(F - F_0)/(F_f - F_0) = K[\text{ligand}]^2/(1 + K[\text{ligand}]^2) \quad (2)$$

F is the fluorescence intensity of the sample. F_0 is the initial fluorescence intensity. F_f is the final fluorescence intensity. a is the asymptotic limit. K_D is the apparent dissociation constant, and K is the apparent binding association constant. It is not unusual to observe binding of more than one ligand to RNA targets, especially in cases in which the small molecule binds with high micromolar K_d.[62−65] This general method for determining binding affinity, in which a change in the conformation of the RNA upon ligand binding results in a change in the fluorescence signal, has been well-established.[13,49,61,66,67] Although some binding events may not be detected by this method, those K_D values that are determined are similar to those measured using other methods. However, the titration of SL3 RNA with six of the molecules, compounds **3**, **8** and **18**−**21**, led to no appreciable change in fluorescence signal. Of these six compounds, four (**18**−**21**) were not investigated further because of their low solubility in water, while the K_D values of the complexes formed between SL3 RNA and compounds **3** and **8** were measured using isothermal titration calorimetry (ITC). The ITC data for the binding of compounds **3** and **8** to SL3 RNA were fit to a sequential two-site binding model (Figure 7). The first and second binding dissociation constants calculated from the ITC data for compound **3** were 11 μM and 11 mM, and for compound **8** they were 68 and 488 μM (Table 1).

Specificity of Identified SL3 Ligands. The specificities of the identified ligands for SL3 RNA over both double- and single-stranded RNAs were determined using fluorescence methods and ITC (Figure 2, Table 2). In the fluorescence studies, both double- and single-stranded RNAs were labeled with fluorescein at the 5′-end and titrated with ligands using procedures similar to those used to measure binding to SL3 RNA. The data were fit to eq 1 assuming 1:1 ligand to RNA binding stoichiometries to determine apparent dissociation constants. Because the addition of **7** to either labeled double- or single-stranded RNA did not lead to significant changes of the fluorescence signal, ITC was used to measure binding. The ITC data for the binding of compound **7** to each of the RNAs were fit to a sequential two-site model. The first and second K_D values calculated from the ITC data for **7** were 189 ± 6 μM and 2.4 ± 2.2 mM for double-stranded RNA and 280 ± 10 μM and 12 ± 2 mM for single-stranded RNA. Titration of **1** and **8** into either double- or single-stranded RNA led to insignificant fluorescence signal changes, and titration of **3** into a solution containing fluorescein alone led to significant signal quenching in a concentration dependent manner. All three compounds have limited solubility at the high concentrations required for ITC assays, and therefore, their binding affinities for double- and single-stranded RNA were not determined.

Among the identified ligands, compounds **7** and **17** are selective for SL3 tetraloop RNA over both double- and single-stranded RNAs. Compound **7** is the most specific and binds 13- and 19-fold better to SL3 RNA than to double- and single-stranded RNAs, respectively. Compound **17** binds >12- and >7-fold better to SL3 RNA than to double- and single-stranded RNAs, respectively. Compounds **14**−**16** bind with similar weak affinity to SL3 RNA and single- and double-stranded RNA and are not included in the table.

Inhibition of SL3−NCp7 Complex Interactions. The ability of the identified SL3 ligands to destabilize the complex formed between SL3 RNA and NCp7 protein was determined using gel mobility shift assays (Figure 8). The data from these assays were fit using eq 3 to determine the IC_{50} values of the NCp7−SL3 complex.

$$B = B_{final} + (B_{initial} - B_{final})/(1 + ([\text{ligand}]/IC_{50})^d) \quad (3)$$

B is the radioactivity (cpm) of the bound RNA observed in the gel, and d is the Hill slope. The apparent inhibition constant (K_i) was calculated from measured IC_{50} values using the following equation:

$$K_i = IC_{50}/(1 + [P_T]/K_D) \quad (4)$$

By use of the data discussed above, the inhibition constants (K_i) of compounds **1**, **3**, **4**, and **8** were calculated to be 110 ± 60 μM, 20 ± 10 μM, 200 ± 100 μM, and 40 ± 1 μM, respectively (Table 3). The observed K_i values of compounds **1**,

dx.doi.org/10.1021/jm2007694 | J. Med. Chem. 2012, 55, 4132−4141

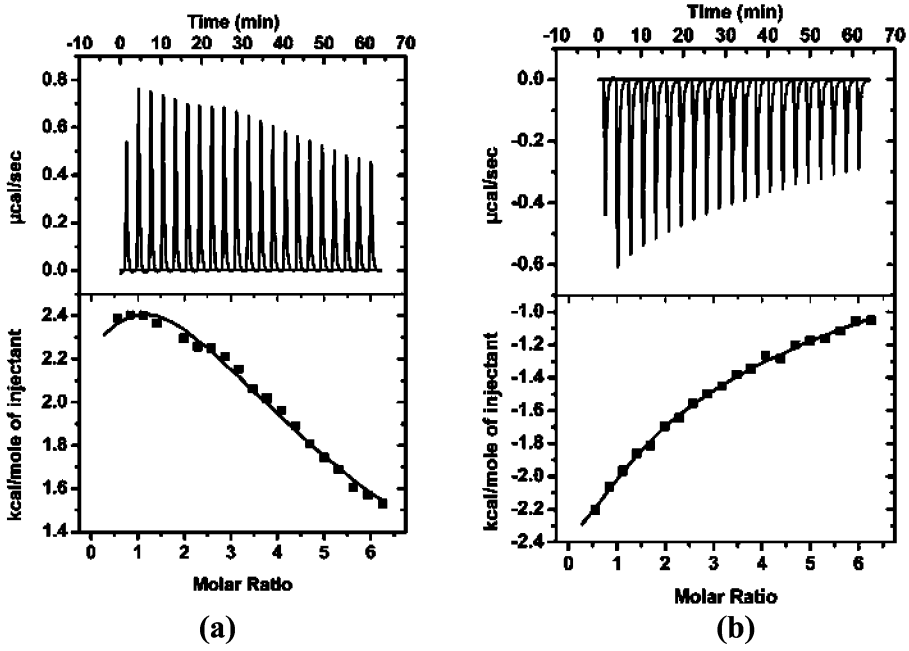

Figure 7. Representative ITC profiles for the titration of (a) **3** and (b) **7** into SL3 RNA. Each heat burst (upper curve) is the result of a 10 μL injection of 1 mM ligand into 20 μM SL3 RNA in 10 mM phosphate buffer, pH 7.4, at 25 °C. The corrected injection heats (bottom curves) were determined from integration of the corresponding heat bursts followed by subtraction of the corresponding dilution heats from control titrations of each ligand into buffer only (data not shown). The data points in the bottom curve are the corrected experimental injection heats, while the continuous line is the calculated fit of the data using a model for two sequential binding sites.

Table 2. Summary of the Apparent Dissociation Constants of the Complexes of Ligands with Different RNA Motifs[a]

	K_D (μM)		
compd	SL3 RNA	double-stranded RNA	single-stranded RNA
4	1.1 ± 0.1	3.2 ± 0.5	2.2
5	3.5 ± 0.3	8.2 ± 0.9	9.5 ± 0.1
6	5.0 ± 0.3	8.3 ± 0.3	11.8 ± 0.3
7[b]	14.5 ± 0.4	189 ± 6	280 ± 10
9	1.7 ± 0.2	2.19 ± 0.01	2.0 ± 0.5
10	4.5 ± 0.9	5.1 ± 0.9	4.1
11	11 ± 2	11.2 ± 0.8	8.9 ± 0.4
12	11.1 ± 0.1	8.4 ± 0.8	14 ± 2
13	13.2 ± 0.3	12 ± 1	7.5 ± 0.1
17	90 ± 10	>1109	>604

[a]Apparent dissociation constants were determined from fluorescence binding measurements. Errors are standard deviation of at least three independent measurements. [b]Dissociation constants determined by ITC. Only dissociation constants for the highest affinity sites from ITC are listed.

3, and **8** are consistent with their respective K_D values for the RNA (Table 1). In contrast, the observed K_i for compound **4** was greater than the K_D of the complex with SL3. This difference between K_i and K_D may be because the destabilization of the NCp7–SL3 RNA complex may require binding of **4** to a second binding site for which it has low affinity or the affinity of **4** for SL3 RNA may be diminished by differences between the buffers used for binding and inhibition assays.

CONCLUSION

By use of both computational and high-throughput screening strategies, 16 compounds that bind SL3 RNA with micromolar affinities have been identified. Ligands **3**–**8** were identified in a similarity search to compound **2** and thus share many structural characteristics. The compounds identified by high throughput screening, compounds **9**–**17**, also share structural characteristics with each other and compounds **3**–**8**, including having conjugated aromatic and heteroaromatic rings linked to functional groups able to participate in hydrogen bonding interactions. Two compounds, **7** and **17**, bind specifically to SL3 RNA compared to single- and double-stranded sequences. The 20-fold specificity exhibited by compound **7** and the greater than 7-fold specificity exhibited by compound **17** are comparable to or better than those of compounds we previously reported.[49] Thus, when taken together with the previous report, we have identified five compounds that bind selectively to SL3 RNA compared to single- or double-stranded RNA. Four of these compounds were identified using computational screening and one by high throughput screening.

Evaluation of all of the SL3 RNA binders identified in this study and the previous report revealed four inhibitors of the SL3–NCp7 complex, **1**, **3**, **4** and **8**, which disrupt the interactions between SL3 RNA and NCp7 protein with 110, 20, 200, and 40 μM inhibition constants, respectively. It is clear that a precise orientation or structural effect on the RNA is required for complex destabilization because most of the compounds that bind the RNA target, even with low micromolar K_D values, do not disrupt the binding of the NCp7 protein. The predicted structures from AutoDock (Figure 5) are consistent with compounds **1**, **3**, **4**, and **8** acting as inhibitors because their predicted binding sites overlap with that of the NCp7 protein. Similarly, the observation that compound **6** does not act as an inhibitor is consistent with its predicted minor groove binding site, which is distant from the binding site of NCp7. However, it is not clear from the modeling why ligands **5** and **7** do not destabilize the complex. Although the high throughput screen identified SL3 RNA binders, no inhibitors of the SL3–NCp7 complex were

dx.doi.org/10.1021/jm2007694 | J. Med. Chem. 2012, 55, 4132–4141

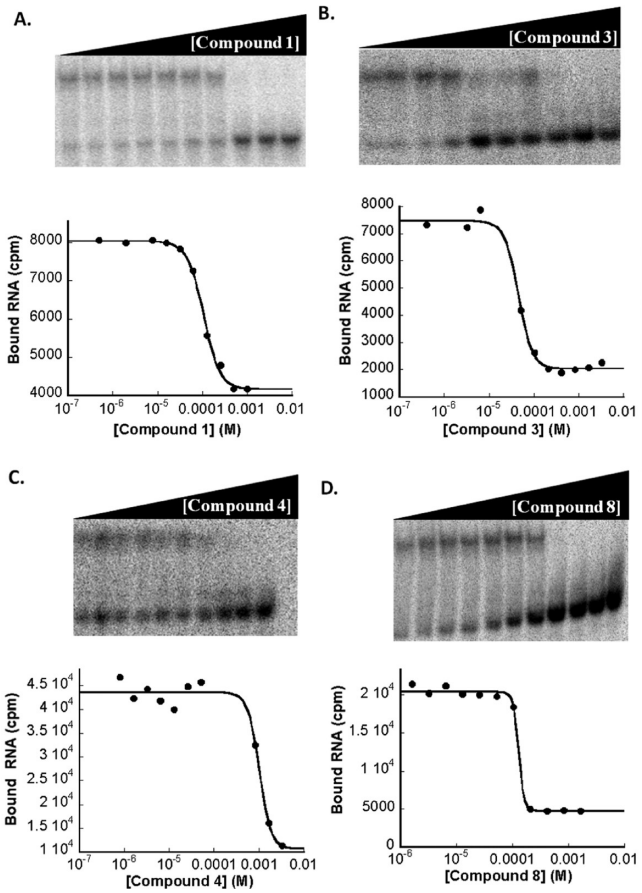

Figure 8. Representative results from gel electrophoresis mobility shift assays showing the displacement of NCp7 from its complex with SL3 RNA by increasing concentrations (left to right) of compounds (A) **1**, (B) **3**, (C) **4**, and (D) **8**. Plots of bound RNA as a function of the concentration of compounds **1**, **3**, **4**, and **8** are shown below each gel mobility shift assay. The data were fit with eq 3 to determine the IC_{50} values.

Table 3. Apparent IC_{50} and K_i for Inhibition of the SL3 RNA–NCp7 Complex by Selected Compounds[a]

compd	IC_{50} (μM)	K_i (μM)
1	340 ± 80	110 ± 60
3	70 ± 30	20 ± 10
4	700 ± 350	200 ± 100
8	123 ± 3	40 ± 1

[a] IC_{50} and K_i values were determined from electrophoresis mobility shift assay experiments. Errors are the standard deviation of at least three independent experiments.

identified with the high throughput screen. It is possible that inhibitors would have been identified if a direct screen of complex destabilization had been performed. However, a direct screen was difficult because many molecules have low solubility under the conditions required for specific binding of the NCp7 protein. Overall, the results suggest that targeted computational docking is an effective method for identifying inhibitors of RNA–protein complexes.

The SL3 ligands identified in this work have not previously been identified as RNA binding compounds and have simple molecular structural identity and low molecular weights, making them ideal for further optimization for the challenging development of high affinity specific ligands for targeting the elements of ψ-RNA of HIV-1. Such compounds have potential applications as anti-HIV-1 agents targeting viral packaging, a critical step in the replication cycle of HIV-1 virus. More generally, these compounds join a small existing pool of small molecule RNA ligands that are able to destabilize RNA–protein complexes.

EXPERIMENTAL SECTION

RNA Sample Preparation. RNA sequences were obtained from Dharmacon Research Inc. (Lafayette, CO). RNA sequences were deprotected and lyophilized following the procedure provided by Dharmacon. The lyophilized RNA samples were desalted by standard ethanol precipitation procedures and their molecular weights confirmed by MALDI mass spectrometry. Before any experiment, the RNA samples were heated at 90–95 °C for 3 min and cooled in ice.

Ligand Samples. All compounds were obtained/purchased in their purest form and confirmed to be >95% pure by HPLC and their identity was confirmed by ESI mass spectrometry unless stated otherwise in the manuscript. Compounds **1** and **2** (Figure 4) were obtained free of charge from the Drug Synthesis and Chemistry Branch, Development Therapeutics Program, Division of Cancer Treatment and Diagnosis, National Cancer Institute (Bethesda, MD). Compound **3** was purchased from Scientific Exchange Inc. (Center Ossipee, NH). Compounds **4**–**21** were purchased from ChemBridge Corporation (San Diego, CA). Ligand stock solutions (10 mM) were prepared in DMSO and diluted in the appropriate buffer for experiments.

High-Throughput Screening. High-throughput screens were performed in the High-Throughput Screening Facility housed in the Department of Chemistry of the University of Illinois. Assays were performed at room temperature. 5′-Fluorescein-labeled SL3 RNA in binding buffer (10 mM Tris-HCl, pH 7.4) was first added to the plates to a final concentration of 10 nM. The initial fluorescence was recorded followed by addition of the small molecules to a final concentration of 1 mM. After incubation for 30 min, the fluorescence was recorded. Molecules that yielded the largest change in fluorescence signal (either increase or decrease) were selected.

Nucleocapsid (NCp7) Sample Preparation. The expression plasmid containing the gene for the NCp7 protein of HIV-1 NL4-3 strain (GenBank accession code AF324493) was a gift from Robert J. Gorelick, AIDS Vaccine Program, SAIC-Frederick, Inc. Plasmid transformation, protein expression in *Escherichia coli* BL21 (DE3) cells, and protein purification followed published procedures.[68] The correct molecular weight of the purified protein was confirmed by MALDI mass spectrometry. The concentration of the protein sample was determined from the UV absorbance at 280 nm using a molar extinction coefficient (ε) of 6050 M^{-1} cm^{-1}.[69] Protein samples were determined to be greater than 95% pure by SDS polyacrylamide gel electrophoresis. Chemically synthesized NCp7 was purchased from GenScript Corp. (Piscataway, NJ). The binding affinity for SL3 RNA of the expressed and the chemically synthesized NCp7 was similar. For both the expressed and chemically synthesized NCp7 samples 1 mM β-mercaptoethanol (BME) and 1 equiv of zinc chloride per Zn^{2+} finger were added. Protein samples were lyophilized and stored at −80 °C. NCp7 protein stock solutions (12 μM) used in the assays were freshly prepared from the lyophilized aliquots in 10 mM Tris-HCl (pH 8.0), 25 mM NaCl, 5 mM $MgCl_2$, 1 mM $ZnCl_2$, 1 mM BME, and 0.01% polyethylene glycol (PEG) buffer, stored at 4 °C and used within 3 days.

Computational Studies. AutoDock4 and AutoDock Tools (ADT) were both obtained from the Molecular Graphics Laboratory of the Scripps Research Institute.[58] Molecular Operating Environment (MOE) from Chemical Computing Group was used to prepare the ligands and to generate their corresponding Protein Data Bank (PDB) file formats. ADT was used for the remainder of the RNA and ligand preparation procedures, including the addition of Gasteiger atomic partial charges. ADT was also used to prepare the input files for both

the AutoGrid and AutoDock programs and for the analysis of the docking results. Virtual molecular dynamics (VMD) was used to visualize the docked structures. All computational procedures involving MOE, AutoDock, ADT, and VMD programs were performed on a desktop PC with a Pentium 4 processor, 3.00 GHz CPU, and 2.00 GB of RAM running Windows XP Professional operating system. The docking site was defined using the program AutoGrid with a grid box of 22.5 Å × 30.0 Å × 26.25 Å (x, y, z) centered at 9.939 Å (x), −5.037 Å (y), and −8.846 Å (z).

Fluorescence Experiments. Fluorescence experiments were performed on a FluoroMax-3 fluorescence spectrometer (Horiba Jobin Yvon). In a standard experiment, 5′-fluorescein-labeled RNA (25 nM) was prepared in fluorescence binding buffer (10 mM Tris-HCl (pH 7.4) and 25 mM NaCl). The RNA sample was excited at 490 nm with a 3 nm band-pass, and the emission fluorescence signal was monitored at 505−530 nm with an 8 nm emission band-pass, while emission at 517 nm was used to determine the K_D. Aliquots (1 μL) of a stock solution of the ligand were sequentially added to the RNA sample at 25 °C until there was no further change in fluorescence signal, allowing 3−5 min for equilibration after each addition. Fluorescence titration data for all compounds were fit to a 1:1 binding model of RNA to ligand using eq 1 except for **1**. Titration data for **1** were fit to a 1:2 binding model of RNA to ligand using eq 2 to calculate the apparent dissociation constants (Tables 1 and 2). Each binding assay was accompanied by a control experiment in which the ligand was titrated into free fluorescein solution. This was performed to exclude the possibility of fluorescence signal changes resulting from the ligand interacting directly with the fluorophore. In addition, a control experiment was performed in which DMSO was added to the RNA solution and no change of the fluorescence signal was observed.

Isothermal Titration Calorimetry (ITC) Assays. In a standard ITC experiment, aliquots of the ligand (10 μL, 1 mM) in 10 mM sodium phosphate (pH 7.4), 10% DMSO buffer were added to the sample cell that contained the RNA (20 μM, 1.42 mL) in the same buffer at 25 °C using a 250 μL rotating syringe (300 rpm). Each experiment was accompanied by a control experiment in which aliquots of the ligand were titrated into buffer alone at 25 °C. The duration of each injection was 24 s, and the spacing between two consecutive injections was 240 s. The initial delay before the first injection was 60 s. Heat absorbed or released for each injection ($\mu cal \cdot s^{-1}$) was measured by determining the area above or under the curve using Origin 5.0 software (MicroCal, Inc., Northampton, MA). The heat of ligand binding for each injection was determined by subtracting ligand-buffer solvation from the heat associated with the corresponding ligand−RNA injection. Dissociation constants were determined by fitting data from plots of heat of ligand binding as a function of ligand−RNA molar ratio to a sequential two-site binding model.

Gel Mobility Shift Assays. Equilibrium dissociation and inhibition constants were measured by gel electrophoresis mobility shift assays. In binding assays, ^{32}P-labeled SL3 RNA (25 pM) was incubated with varying amounts of NCp7 at 25 °C for 1 h in buffer containing 50 mM Tris-HCl (pH 7.4), 40 mM $MgCl_2$, 200 mM NaCl, 0.1 mM $ZnCl_2$, 5% glycerol, and 1% (v/v) BME. The bound and free RNAs were separated using a 6% polyacrylamide gel in 50 mM Tris-borate, pH 8.0, and 0.1% Triton-X 100 for 1 h at 300 V at 4 °C. Gels were visualized on a Molecular Dynamics Storm imager. Fraction of RNA bound versus protein concentration was plotted, and the data were fit using the equation $y = 1/(1 + K_D/[P]_T)$ in which y is the fraction of RNA bound, K_D is the equilibrium dissociation constant, and $[P]_T$ is the total protein concentration. All binding measurements were performed with greater than 10-fold excess of protein over RNA so that $[P]$ was approximately equal to $[P]_T$.

In inhibition assays, the RNA−protein complex was preformed by incubating ^{32}P-labeled SL3 RNA (25 pM) with NCp7 (75 nM) at 25 °C for 1 h in binding buffer as described above. The ligand from the stock solution was added, and the solution was incubated for an additional 1 h. Each inhibition experiment was accompanied by a control experiment in which DMSO equal to the highest concentration used in inhibition assays was added into the RNA−protein complex. The samples were loaded onto a 6% polyacrylamide gel for separation as described for the binding assays. The data were fit using eq 3 to determine the IC_{50} values and eq 4 to calculate the inhibition constants. Representative gel shift mobility assays and plots are shown in Figure 8. Inhibition constants are listed in Table 3.

■ ASSOCIATED CONTENT

Ⓢ Supporting Information

Analysis of ligand binding conformations and illustrations of strategies in virtual and high-throughput screening identification of ligands. This material is available free of charge via the Internet at http://pubs.acs.org.

■ AUTHOR INFORMATION

Corresponding Author

*Phone: (510) 642-0336. Fax: (217) 244-8024. E-mail: abaranger@berkeley.edu.

Notes

The authors declare no competing financial interest.

■ ACKNOWLEDGMENTS

Compounds **1** and **2** were provided by the National Cancer Institute. The expression plasmid for the NCp7 protein was a gift from Dr. Robert J. Gorelick, AIDS Vaccine Program, SAIC-Frederick, Inc. We are thankful to Dr. Karin Musier-Forsyth of The Ohio State University for assistance with the NCp7 protein expression and purification protocol.

■ REFERENCES

(1) Brisson-Noel, A.; Trieu-Cuot, P.; Courvalin, P. Mechanism of action of spiramycin and other macrolides. *Chemotherapy* **1988**, *22* (Suppl. B), 13−23.

(2) Heinz, B. A.; McKinght, K. l. RNA as a target for developing antivirals. *Antiviral Chem. Chemother.* **2003**, *14*, 61−73.

(3) Cheng, A. C.; Calabro, V.; Frankel, A. D. Design of RNA-binding proteins and ligands. *Curr. Opin. Struct. Biol.* **2001**, *11*, 478−484.

(4) DeJong, E. S.; Luy, B.; Marino, J. P. RNA and RNA−protein complexes as targets for therapeutic intervention. *Curr. Top. Med. Chem* **2002**, *2*, 289−302.

(5) Schroeder, R.; Barta, A.; Semrad, K. Strategies for RNA folding and assembly. *Nat. Rev. Mol. Cell Biol.* **2004**, *5*, 908−919.

(6) Sevignani, C.; Calin, G. A.; Siracusa, L. D.; Crose, C. M. Mammalian microRNAs: a small world for fine-tuning gene expression. *Mamm. Genome* **2006**, *17*, 189−202.

(7) Vicens, Q.; Westhof, E. RNA as a drug target: the case of aminoglycosides. *ChemBioChem* **2003**, *4*, 1018−1023.

(8) Winkler, W. C.; Breaker, R. R. Genetic control by metabolite-binding riboswitches. *ChemBioChem* **2003**, *4*, 1024−1032.

(9) Bélanger, F.; Gagnon, M. G.; Steinberg, S. V.; Cunningham, P. R.; Brakier-Gingras, L. Study of the functional interaction of the 900 tetraloop of 16S ribosomal RNA with helix 24 within the bacterial ribosome. *J. Mol. Biol.* **2004**, *338*, 683−693.

(10) Bozdogan, B.; Appelbaum, P. C. Oxazolidinones: activity, mode of action, and mechanism of resistance. *Int. J. Antimicrob. Agents* **2004**, *23*, 113−119.

(11) Brodersen, D. E.; Clemons, W. M. J.; Carter, A. P.; Morgan-Warren, R. J.; Wimberly, B. T.; Ramakrishnan, V. The structural basis for the action of the antibiotics tetracycline, pactamycin, and hygromycin B on the 30S ribosomal subunit. *Cell* **2000**, *103*, 1143−1154.

(12) Tor, Y. The ribosomal A-site as an inspiration for the design of RNA binders. *Biochimie* **2006**, *88*, 1045−1051.

(13) Thomas, J. R.; Hergenrother, P. J. Targeting RNA with small molecules. *Chem. Rev.* **2008**, *108*, 1171−1224.

(14) Lee, M. M.; Pushechnikov, A.; Disney, M. D. Rational and modular design of potent ligands targeting the RNA that causes myotonic dystrophy 2. *ACS Chem. Biol.* **2009**, *4*, 345−355.
(15) Pushechnikov, A.; Lee, M. M.; Childs-Disney, J. L.; Sobczak, K.; French, J. M.; Thornton, C. A.; Disney, M. D. Rational design of ligands targeting triplet repeating transcripts that cause RNA dominant disease: application to myotonic muscular dystrophy type 1 and spinocerebellar ataxia type 3. *J. Am. Chem. Soc.* **2009**, *131*, 9767−9779.
(16) Lee, M. M.; Childs-Disney, J. L.; Pushechnikov, A.; French, J. M.; Sobczak, K.; Thornton, C. A.; Disney, M. D. Controlling the specificity of modularly assembled small molecules for RNA via ligand module spacing: targeting the RNAs that cause myotonic muscular dystrophy. *J. Am. Chem. Soc.* **2009**, *131*, 17464−17472.
(17) Tibodeau, J. D.; Fox, P. M.; Ropp, P. A.; Theil, E. C.; Thorp, H. H. The up-regulation of ferritin expression using a small-molecule ligand to the native mRNA. *Proc. Natl. Acad. Sci. U.S.A.* **2006**, *103*, 253−257.
(18) Kirk, S. R.; Luedtke, N. W.; Tor, Y. Neomycin−acridine conjugate: a potent inhibitor of Rev-RRE binding. *J. Am. Chem. Soc.* **2000**, *122*, 980−981.
(19) Gayle, A. Y.; Baranger, A. M. Inhibition of the U1A-RNA complex by an aminoacridine derivative. *Bioorg. Med. Chem. Lett.* **2002**, *12*, 2839−2842.
(20) Manfroni, G.; Gatto, B.; Tabarrini, O.; Sabatini, S.; Cecchetti, V.; Giaretta, G.; Parolin, C.; Vecchio, C. D.; Calistri, A.; Palumbo, M.; Fravolini, A. Synthesis and biological evaluation of 2-phenylquinolones targeted at Tat/TAR interaction. *Bioorg. Med. Chem. Lett.* **2009**, *19*, 714−717.
(21) Gareiss, P. C.; Sobczak, K.; McNaughton, B. R.; Palde, P. B.; Thornton, C. A.; Miller, B. L. Dynamic combinatorial selection of molecules capable of inhibiting the (CUG) repeat-MBNL1 interaction in vitro: discovery of lead compounds targeting myotonic dystrophy (DM1). *J. Am. Chem. Soc.* **2008**, *130*, 16254−16261.
(22) Galicia-Vazquez, G.; Lindqvist, L.; Wang, X.; Harvey, I. High-throughput assays probing protein−RNA interactions of eukaryotic translation initiation factors. *Anal. Biochem.* **2009**, 384.
(23) Arambula, J. F.; Ramisetty, R. R.; Baranger, A. M.; Zimmerman, S. C. A simple ligand that selectively targets CUG trinucleotide repeats and inhibits MBNL protein binding. *Proc. Natl. Acad. Sci. U.S.A.* **2009**, *106*, 16068−16073.
(24) Warf, M. B.; Nakamori, M.; Matthys, C. M.; Thornton, C. A.; Berglund, J. A. Pentamidine reverses the splicing defects associated with myotonic dystrophy. *Proc. Natl. Acad. Sci. U.S.A.* **2009**, *106*, 18551−18556.
(25) Wang, D.; Iera, J.; Baker, H.; Hogan, P.; Ptak, R.; Yang, L.; Hartman, T.; Buckheit, R. W.; Desjardins, A.; Yang, A.; Legault, P.; Yedavalli, V.; Jeang, K.-T.; Apella, D. H. Multivalent binding oligomers inhibit HIV Tat-TAR interaction critical for viral replication. *Bioorg. Med. Chem.* **2009**, *19*, 6893−6897.
(26) Xiao, G.; Kumar, A.; Li, K.; Rigle, C. T.; Bajic, M.; Davis, T. M.; Boykin, D. W.; Wilson, W. D. Inhibition of the HIV-1 Rev-RRE complex formation by unfused aromatic cations. *Bioorg. Med. Chem.* **2001**, *9*, 1097−1113.
(27) Schirle, N. T.; Goodman, R. A.; Krishnamurthy, M.; Beal, P. A. Selective inhibition of ADAR2-catalyzed editing of the serotonin 2c receptor pre-mRNA by a helix-threading peptide. *Org. Biomol. Chem.* **2010**, *8*, 4898−4904.
(28) Bugaut, A.; Rodriguez, R.; Kumari, S.; Hsu, D. S.-T.; Balasubramanian, S. Small molecule-mediated inhibition of translation by targeting a native RNA G-quadruplex. *Org. Biomol. Chem.* **2010**, *8*, 2771−2776.
(29) Gatto, B.; Tabarrini, O.; Massari, S.; Giaretta, G.; Sabatini, S.; Vecchio, C. D.; Parolin, C.; Fravolini, A.; Palumbo, M.; Cecchetti, V. 2-Phenylquinolones as inhibitors of the HIV-1 Tat-TAR interaction. *ChemMedChem* **2009**, *4*, 935−938.
(30) Turner, K. B.; Hagan, N. A.; Fabris, D. Inhibitory effects of archetypical nucleic acid ligands on the interactions of HIV-1 nucleocapsid protein with elements of psi-RNA. *Nucleic Acids Res.* **2006**, *34*, 1305−1316.
(31) Amarasinghe, G. K.; De Guzman, R. N.; Turner, R. B.; Chancellor, K. J.; Wu, Z. R.; Summers, M. F. NMR structure of the HIV-1 nucleocapsid protein bound to stem-loop SL2 of the Psi-RNA packaging signal. Implications for genome recognition. *J. Mol. Biol.* **2000**, *301*, 491−511.
(32) Darlix, E.-L.; Lapadat-Tapolsky, M.; Rocquigny, H. D.; Roques, B. P. First glimpses at structure−function relationships of the nucleocapsid protein of retroviruses. *J. Mol. Biol.* **1995**, *254*, 523−537.
(33) Dietz, J. K., J.; Kaur, A.; Raja, C.; Stein, S.; Grez, M.; Pustowka, A.; Mensch, S.; Ferner, J.; Möller, L.; Bannert, N.; Tampé, R.; Divita, G.; Mély, Y.; Schwalbe, H.; Dietrich, U. Inhibition of HIV-1 by a peptide ligand of the genomic RNA packaging signal psi. *ChemMedChem* **2008**, *3*, 749−755.
(34) Chadwick, D. R.; Lever, A. M. Antisense RNA sequences targeting the 5′ leader packaging signal region of human immunodeficiency virus type-1 inhibits viral replication at post-transcriptional stages of the life cycle. *Gene Ther.* **2000**, *7*, 1362−1368.
(35) Clever, J.; Sassetti, C.; Parslow, T. G. RNA secondary structure and binding sites for gag gene products in the 5′ packaging signal of human immunodeficiency virus type 1. *J. Virol.* **1995**, *69*, 2101−2109.
(36) Clever, J. L.; Eckstein, D. A.; Parslow, T. G. Genetic dissociation of the encapsidation and reverse transcription functions in the 5′ R region of human immunodeficiency virus type 1. *J. Virol.* **1999**, *73*, 101−109.
(37) Clever, J. L.; Parslow, T. G. Mutant human immunodeficiency virus type 1 genomes with defects in RNA dimerization or encapsidation. *J. Virol.* **1997**, *71*, 3407−3414.
(38) Damgaard, C. K.; Dyhr-Mikkelsen, H.; Kjems, J. Mapping the RNA binding sites for human immunodeficiency virus type-1 Gag and NC proteins within the complete HIV-1 and -2 untranslated leader regions. *Nucleic Acids Res.* **1998**, *26*, 3667−3676.
(39) Hayashi, T.; Shioda, T.; Iwakura, Y.; Shibuta, H. RNA packaging signal of human immunodeficiency virus type 1. *Virology* **1992**, *188*, 590−599.
(40) McBride, M. S.; Panganiban, A. T. The human immunodeficiency virus type 1 encapsidation site is a multipartite RNA element composed of functional hairpin structures. *J. Virol.* **1996**, *70*, 2963−2973.
(41) McBride, M. S.; Panganiban, A. T. Position dependence of functional hairpins important for human immunodeficiency virus type 1 RNA encapsidation in vivo. *J. Virol.* **1997**, *71*, 2050−2058.
(42) McBride, M. S.; Schwartz, M. D.; Panganiban, A. T. Efficient encapsidation of human immunodeficiency virus type 1 vectors and further characterization of cis elements required for encapsidation. *J. Virol.* **1997**, *71*, 4544−4554.
(43) Michael, F. S.; Andrew, C. P.; Bruce, S. H.; Philip, N. B. Affinities of packaging domain loops in HIV-1 RNA for the nucleocapsid protein. *Biochemistry* **2002**, *41*, 5276−5282.
(44) Dorman, M. N.; Lever, A. M. L. Investigation of RNA transcripts containing HIV-1 packaging signal sequences as HIV-1 antivirals: generation of cell lines resistant to HIV-1. *Gene Ther.* **2001**, *8*, 157−165.
(45) Jenkins, L. M. M.; Byrd, J. C.; Hara, T.; Srivastava, P.; Mazur, S. J.; Stahl, S. J.; Inman, J. K.; Appella, E.; Omichinski, J. G.; Legault, P. Studies on the mechanism of inactivation of the HIV-1 nucleocapsid protein NCp7 with 2-mercaptobenzamide thioesters. *J. Med. Chem.* **2005**, *48*, 2847−2858.
(46) Paillart, J.-C.; Shehu-Xhilaga, M.; Marquet, R.; Mak, J. Dimerization of retroviral RNA genomes: an inseparable pair. *Nat. Rev. Microbiol.* **2004**, *2*, 461−472.
(47) Rice, W. G.; Supko, J. G.; Malspeis, L.; Buckheit, R. W.; Clanton, D.; Bu, M.; Graham, L.; Schaeffer, C. A.; Turpin, J. A.; Domagala, J.; Gogliotti, R.; Bader, J. P.; Halliday, S. M.; Coren, L.; Sowder, R. C.; Arthur, L. O.; Henderson, L. E. Inhibitors of HIV nucleocapsid protein zinc fingers as candidates for the treatment of AIDS. *Science* **1995**, *270*, 1194−1197.
(48) Skripkin, E.; Paillart, J.-C.; Marquet, R.; Blumenfeld, M.; Ehresmann, B.; Ehresmann, C. Mechanisms of inhibition of in vitro

dimerization of HIV type I RNA by sense and antisense oligonucleotides. *J. Biol. Chem.* **1996**, *271*, 28812−28817.
(49) Warui, D. M.; Baranger, A. M. Identification of specific small molecule ligands for stem loop 3 ribonucleic acid of the packaging signal psi of human immunodeficiency virus-I. *J. Med. Chem.* **2009**, *52*, 5462−5473.
(50) Yan, Z.; Sikri, S.; Beveridge, D. L.; Baranger, A. M. Identification of an aminoacridine derivative that binds to RNA tetraloops. *J. Med. Chem.* **2007**, *50*, 4096−4104.
(51) Haddad, J.; Kotra, L. P.; Liano-Sotelo, B.; Kim, C.; Azucena, E. F.; Liu, M.; Vakulenko, S. B.; Chow, C. S.; Mobashery, S. Design of novel antibiotics that bind to the ribosomal acyltransfer site. *J. Am. Chem. Soc.* **2002**, *124*, 3229−3237.
(52) Barbault, F.; Zhang, L.; Zhang, L.; Fan, B. T. Parametrization of a specific free energy function for automated docking against RNA targets using neural networks. *Chem. Intell. Lab. Syst.* **2006**, *82*, 269−275.
(53) Chen, Q.; Kuntz, I. D.; Shafer, R. H. Structure-Based Design of Nucleic Acid Binding Drugs. In *Structure, Motion, Interaction and Expression of Biological Macromolecules*; Adenine Press: New York, 1997; pp 227−231.
(54) Detering, C.; Varani, G. Validation of automated docking programs for docking and database screening against RNA drug targets. *J. Med. Chem.* **2004**, *47*, 4188−4201.
(55) Evans, D. A.; Neidle, S. Virtual screening of DNA minor groove binders. *J. Med. Chem.* **2006**, *49*, 4232−4238.
(56) Moitessier, N.; Westhof, E.; Hanessian, S. Docking of aminoglycosides to hydrated and flexible RNA. *J. Med. Chem.* **2006**, *49*, 1023−1033.
(57) Zhang, X.; Wang, X.; Liu, C. Molecular docking and 3D-QSAR study of pyranmycin derivatives against 16S rRNA A site. *J. Mol. Struct.: THEOCHEM* **2005**, *730*, 85−94.
(58) Morris, G. M.; Goodsell, D. S.; Halliday, R. S.; Huey, R.; Hart, W. E.; Belew, R. K.; Olson, A. J. Automated docking using a Lamarckian genetic algorithm and an empirical binding free energy function. *J. Comput. Chem.* **1998**, *19*, 1639−1662.
(59) De Guzman, R. N.; Wu, Z. R.; Stalling, C. C.; Pappalardo, L.; Borer, P. N.; Summers, M. F. Structure of the HIV-1 nucleocapsid protein bound to the SL3 psi-RNA recognition element. *Science* **1998**, *249*, 384−388.
(60) Liu, X.; Thomas, J. R.; Hergenrother, P. J. Deoxystreptamine dimers bind to RNA hairpin loops. *J. Am. Chem. Soc.* **2004**, *126*, 9196−9197.
(61) Thomas, J. R.; Liu, X.; Hergenrother, P. J. Size-specific ligands for RNA hairpin loops. *J. Am. Chem. Soc.* **2005**, *127*, 12434−12435.
(62) Ramisetty, S. R.; Baranger, A. M. Cooperative binding of a quinoline derivative to an RNA stem loop containing a dangling end. *Bioorg. Med. Chem. Lett.* **2010**, *20*, 3134−3137.
(63) Shen, L. L.; Mitscher, L. A.; Sharma, P. N.; O'Donnell, T. J.; Chu, D. W. T.; Cooper, C. S.; Rosen, T.; Pernet, A. G. Mechanism of inhibition of DNA gyrase by quinolone antibacterials: a cooperative drug−DNA binding model. *Biochemistry* **1989**, *28*, 3886−3894.
(64) Kwon, M.; Strobel, S. A. Chemical basis of glycine riboswitch cooperativity. *RNA* **2008**, *14*, 25−34.
(65) Mandal, M.; Lee, M.; Barrick, J. E.; Weinberg, Z.; Emilsson, G. M.; Ruzzo, W. L.; Breaker, R. R. A glycine-dependent riboswitch that uses cooperative binding to control gene expression. *Science* **2004**, *306*, 275−279.
(66) Llano-Sotelo, B.; Azucena, E.; Kotra, L.; Mobashery, S.; Chow, C. Aminoglycosides modified by resistance enzymes display diminished binding to the bacterial ribosomal aminoacyl-tRNA site. *Chem. Biol.* **2002**, *9*, 455−463.
(67) Llano-Sotelo, B.; Chow, C. S. RNA-aminoglycoside antibiotic interactions: fluorescence detection of binding and conformational change. *Bioorg. Med. Chem. Lett.* **1999**, *8*, 213−216.
(68) Carteau, S. G.; R., J.; Bushman, F. D. Coupled integration of human immunodeficiency virus type 1 cDNA ends by purified integrase in vitro: stimulation by the viral nucleocapsid protein. *J. Virol.* **1999**, *73*, 6670−6679.
(69) Stewart-Maynard, K. M.; Cruceanu, M.; Wang, F.; Vo, M.-N.; Gorelick, R. J.; Williams, M. C.; Rouzina, I.; Musier-Forsyth, K. Retroviral nucleocapsid proteins display nonequivalent levels of nucleic acid chaperone activity. *J. Virol.* **2008**, *82*, 10129−10142.